Data in Brief 33 (2020) 106443

Contents lists available at ScienceDirect

Data in Brief

journal homepage: www.elsevier.com/locate/dib

Data Article

Single tracks data obtained by selective laser melting of Ti6Al4V with a small laser spot diameter

Emanuele Vaglio, Thomas De Monte, Alex Lanzutti, Giovanni Totis*, Marco Sortino, Lorenzo Fedrizzi

Polytechnic Department of Engineering and Architecture, University of Udine, Via delle Scienze 206, Udine 33100, Italy

ARTICLE INFO

Article history:
Received 25 September 2020
Revised 15 October 2020
Accepted 16 October 2020
Available online 22 October 2020

Keywords:
Selective laser melting
Titanium Ti6Al4V
Small laser spot diameter
Single track analysis

ABSTRACT

Nowadays, advanced metal components with high geometrical complexity can be 3D printed by using the Selective Laser Melting (SLM) technology. Despite SLM resolution and accuracy are generally limited to some tenths of mm, it should be possible to produce finer and more precise details by applying lasers with a small spot diameter. However, to present date the data collected with small laser spot diameters are poor. In this work, experimental data describing the effects of laser power and scan speed on single track formation when applying a small laser spot diameter of 50 µm on Ti6Al4V powder are reported. SEM images and the extracted geometrical data characterizing the obtained single tracks are provided here, as well as their microstructural analysis and microhardness measurements.

* Corresponding author.
E-mail address: giovanni.totis@uniud.it (G. Totis).

https://doi.org/10.1016/j.dib.2020.106443

Specifications Table

Subject	Industrial and Manufacturing Engineering
Specific subject area	Additive Manufacturing, Metal Powder Bed Fusion, Selective Laser Melting
Type of data	Tables, Images, Charts (e.g. statistical boxplots), Graphs and Figures
How data were acquired	SEM, Optical Microscope, Micro-hardness measurement device
Data format	Raw and Analyzed
Parameters for data collection	Single track morphological classification and geometrical characterization (e.g. track width, height and depth) was carried out by varying laser power and scanning speed; cross-section micro-hardness was measured at different inspection points located beneath the single track.
Description of data collection	Single tracks were selectively melted on a layer of Titanium Ti6Al4V powder by using a laser spot diameter of 50 µm. An industrial 3D printing machine Concept Laser M2 Cusing was used. Process parameters were varied according to a 8×10 full factorial design of experiments.
Data source location	Institution: LAMA FVG laboratory, Polytechnic Department of Engineering and Architecture, University of Udine, 33100 Udine, Italy
Data accessibility	Data are available within this article and at the Mendeley Repository at https://data.mendeley.com/datasets/s9438vb5xd/draft?a=4fd639be-e2c9-4d2b-8c3b-1240a8918b5f

Value of the Data

- The experimental data can be used for a straightforward optimization of process parameters when applying a laser spot diameter of about 50 µm for the Selective Laser Melting of Ti6Al4V powder.
- Industrial process engineers and researchers working in this field may benefit from these data.
- The SEM images illustrating top and cross-section views of the single tracks can be used to train and validate some innovative methodologies for the automatic analysis of track morphology.
- SEM images and track geometrical features can be used to develop and validate novel techniques for automatic detection or for a priori prediction of different process anomalies (e.g. keyhole formation, balling, spattering, etc.) that may negatively impact the printing process of real 3D parts.
- Accordingly, these data can be used to train or validate some novel analytical and numerical methods for process parameters optimization in SLM.

1. Data Description

1.1. Data summary

With the aim of improving the capability of 3D printing small and accurate geometrical details, the layer thickness as well as the laser spot diameter should be minimized by concurrently optimizing the laser power P and the scanning speed v [1,5].

Nevertheless, the application of small laser spot diameters in conventional Selective Laser Melting (i.e. by excluding the special micro SLM conditions, such as those illustrated in [3]) has been little investigated to present date.

For instance, a laser spot diameter of about 70 µm was applied for studying single tracks formation on alloyed steels [2,8,9], on Nickel-based alloys [9][4] and on the aluminium AlSi10Mg alloy [6].

However, the extra-low-interstitial grade of Ti6Al4V alloy is of particular relevance in many strategic industrial sectors such as biomedical, aerospace, automotive and energy. Most applications in these industrial fields require very small and complex geometric features. In 2018 Xiang et al. [7] investigated single tracks' formation on this material by adopting a laser spot diameter of 80 µm. Up to authors' knowledge, no other accessible literature covering smaller laser spot diameters on this Titanium grade is available.

Therefore, data reported here are of crucial importance since they were obtained on Ti6Al4V by using a laser spot diameter of 50 µm. They were collected according to a full factorial design of experiments consisting in single tracks scanning. Process conditions, measurement devices and procedures are detailed in the next section. Design factors were the laser power P (8 levels in the range $50 \div 400$ W) and the scan speed v (10 levels in the range $250 \div 2500$mm/s).

Basically, the data provided here are as follows.

1. Process conditions and raw materials data – such as powder characteristics – that are reported in the next section.
2. Raw SEM images of single tracks top and cross-section views, for their morphological and geometrical characterization. Process parameters are codified in the file name according to the format "P_v.jpg", where P is the laser power in W and v is the scan speed in mm/s.
3. Single tracks geometrical features derived from the analysis of SEM images are provided as Excel tables that can be found at the Mendely link reported above. Whenever possible, for each track and for each geometrical feature 3 measurements were taken at different locations along the track in order to determine an average value that was finally reported in the table. The same average values were also represented by using statistical boxplots and finally compared with simple interpolating models for showing their random properties.
4. Micro-hardness values are also provided in the same Excel file described above, and they are further illustrated by means of statistical boxplots in this section.

1.2. Morphological classification data of single tracks

Single tracks were firstly analyzed to determine their morphology, and then metallographic analysis and dimensional measurement of their cross sections were carried out.

Single track scanning is schematically illustrated in Fig. 1. An example of single track top and cross section views is given in Fig. 2, where most of the typical defects affecting track morphology are visible.

Different kinds of single track morphology were obtained here, that are illustrated in Fig. 3(a). Specifically, the tracks were classified into five distinct categories according to their morphology, as follows:

1. Strongly discontinuous (I): the track was absent or only some isolated solidified drops – caused by the balling phenomenon – were found.
2. Discontinuous (II): a partial track formation was achieved owing to a slightly higher energy density.
3. Continuous but irregular (III): substrate alteration was continuous; however, the resulting track was strongly jagged. Moreover, at low laser power levels, many partially melted particles were found near the track.
4. Regular and thin (IV): the track was continuous and predominantly regular. Track width was about twice the laser spot diameter. A high-power level combined with medium-to-low scanning speeds promoted a stable melt pool.
5. Regular and thick (V): the track was continuous and regular like in the previous case; however, its width was higher and its depth was much deeper because of the higher energy density. Tracks were affected by the typical keyhole porosity owing to excessive material evaporation. The effects of flows inside the melt pool can been seen in the top views.

The process parameters map obtained here is reported in Fig. 3(b). As done in recent research works [7], single track results can be roughly classified by using the linear energy density, which

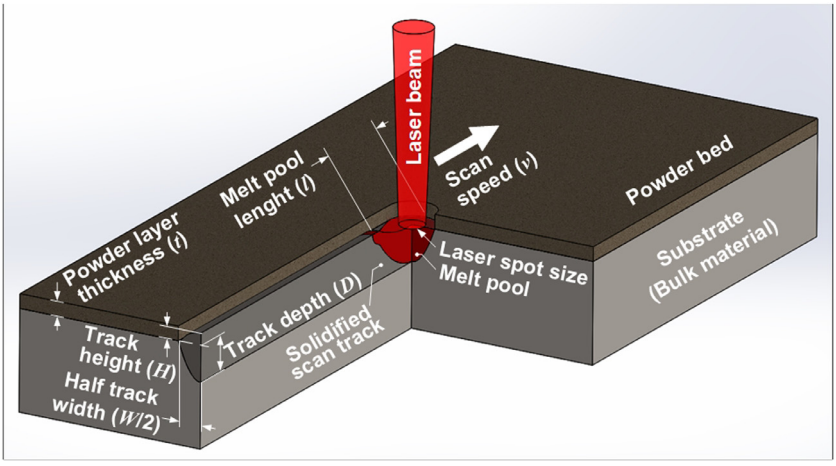

Fig. 1. Single track dimensions.

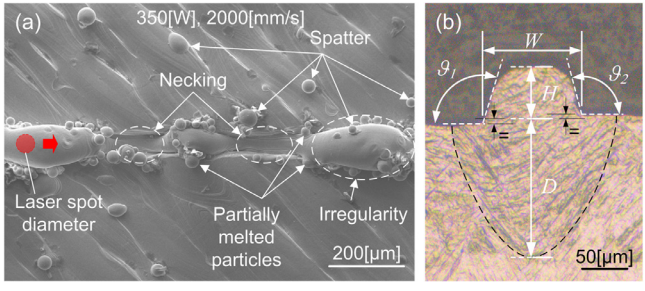

Fig. 2. Single track morphology. Top view with typical defects (a) and cross section measurements (b), where the Heat Affected Zone is also visible.

is given by

$$ED_L = P/v, \tag{1}$$

where P is the laser power and v is the scanning speed.

From the results presented in Fig. 3, no track or a strongly discontinuous track was formed (categories I and II) when ED_L was less than 0.05 J/mm owing to the insufficient amount of energy transferred to the powder and to the balling phenomenon.

For ED_L levels in the range between 0.10 J/mm and 0.20 J/mm (category III), several morphological defects were found, as shown in Figure 2. Specifically, single tracks of category III were affected by irregularities and necking. Partially melted powders together with spatter generation were also observed under these conditions.

On the other hand, continuous and regular shapes can be observed for ED_L values between 0.20 J/mm and 0.40 J/mm, whereas above 0.40 J/mm a substantial evaporation of materials takes place. This enhances the energy absorption of the laser source, thus causing an excessive track penetration. In addition, vapor cavity collapses during the cooling phase and typical keyhole voids can be seen in the cross-section views.

This gives rise to single tracks of category V. From the top views, the only visible difference between category IV and category V is the considerably greater thickness of the tracks belonging to the latter category.

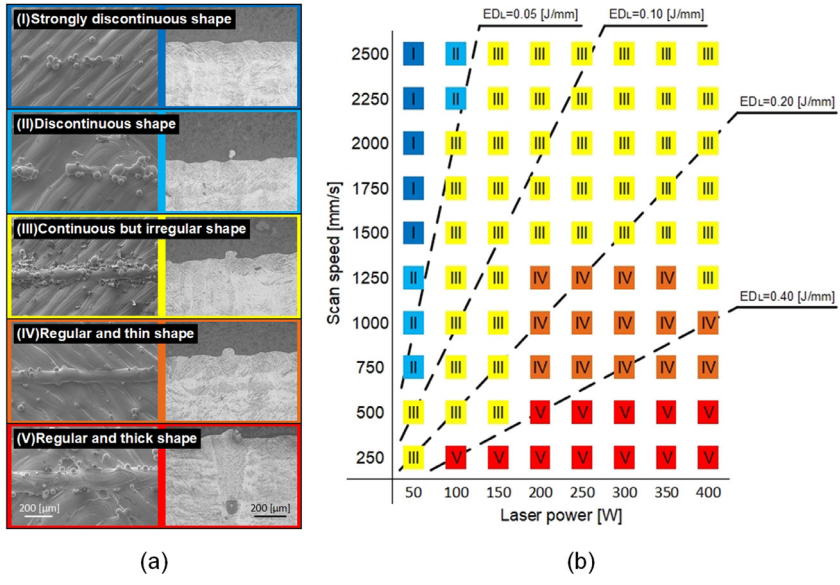

Fig. 3. (a) Examples of the top and cross-section views of single tracks and (b) process map obtained.

In short, the best single tracks were found when $0.20 \leq ED_L \leq 0.40$J/mm. However, this window does not ensure an adequate 3D printing of bulk parts because of the expected heat accumulation effects in the presence of multi-track and multi-layer configuration. Process parameters corresponding to lower energy densities – from 0.1 to 0.2 J/mm – should be considered as the best candidates for a successful 3D printing.

1.3. Track geometry measurements

From the analysis of SEM images the following characteristics were determined: the track width W, height H, depth D and contact angle ϑ were determined that are defined in Fig. 2(b). Statistical boxplots showing the behavior of the observed quantities are reported in Figure 4. The analysis of variance was carried out in order to determine the most important dependencies between the observed variables and the process parameters. Eventually, the interpolating models reprsented in Fig. 5 were determined through the stepwise regression algorithm that was executed both in natural and logarithmic scale. The results from the analysis of variance and from linear regression are reported in Table 1.

1.4. Microstructure

Metallographic analysis was also carried out in order to achieve a complete physical characterization of the single tracks and of the underlying substrate. As it is visible in Fig. 2(b), the microstructure was fully composed of Ti martensite. This indicates that the material underwent high cooling rates during and after the solidification. The formation of martensite was likely due to the high difference between the volume of the single track and the volume of the base that was already solidified when the single track study was carried out. The microstructure did not depend on the process parameters, and no secondary phases generated by the reheating of the material were detected in the Heat-Affected Zones.

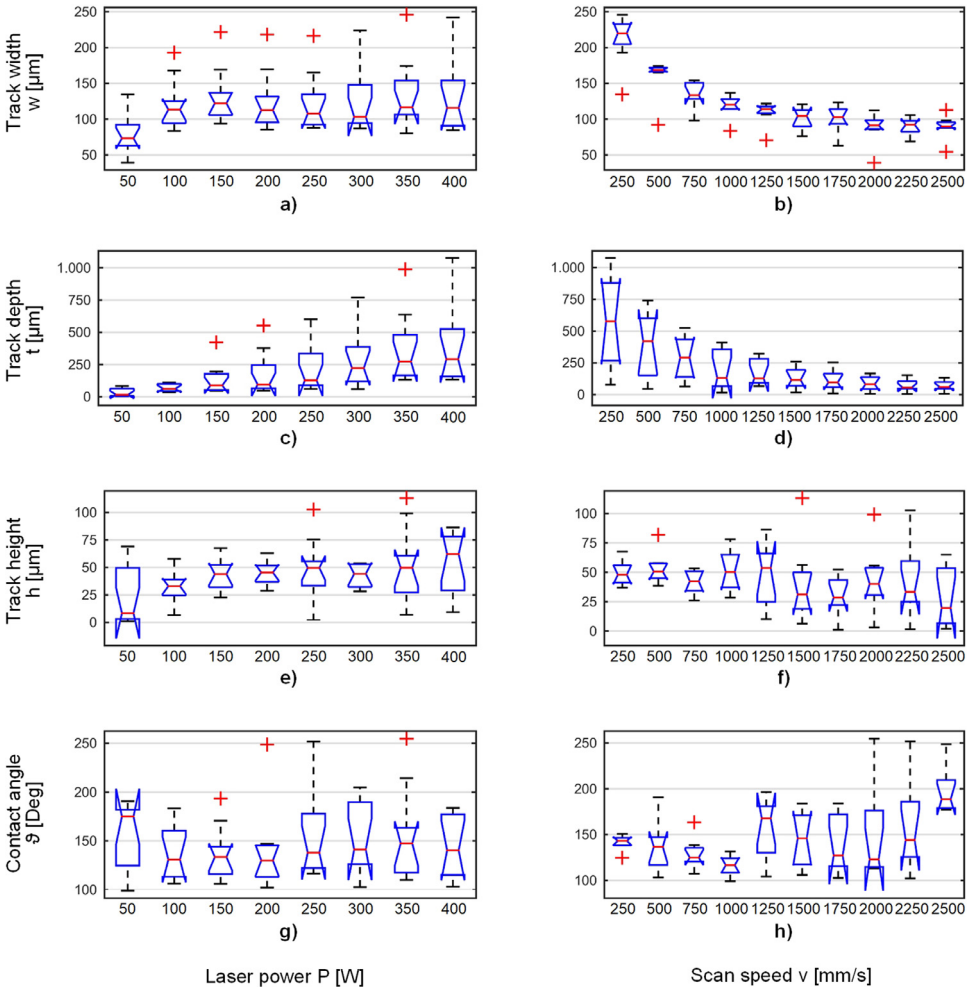

Fig. 4. Box plot of single track width (a,b), depth (c,d), height (e,f), and contact angle (g,h) at different laser power and scanning speed levels.

Table 1
Analysis of variance and interpolating models of the geometric features. μ_ε and σ_ε are the systematic and random relative errors, respectively.

	ANOVA (p-value)					
Geometric feature	P [W]	v [mm/s]	Model	$\mathbf{R^2}$	μ_ϵ[%]	σ_ϵ[%]
Track width	7.59e−15	1.95e−32	$645P^{0.2}v^{-0.4}$	0.90	9	11.4
Track depth	2.29e−11	1.91e−14	$120.3P^{1.3}v^{-1}$	0.94	18	31.9
Track height	0.071	0.3296	$26.7 + 7.2 \cdot 10^{-2}P$	0.13	38.8	50.3
Contact angle	0.4455	0.0004	$126.8 + 8.14 \cdot 10^{-6}v^2$	0.20	18.2	22.4

1.5. Microhardness

The microhardness analysis was carried out by considering only the samples obtained with a laser power of 200 W, 300 W and 350 W with a scanning speed of 250 mm/s, 500 mm/s and

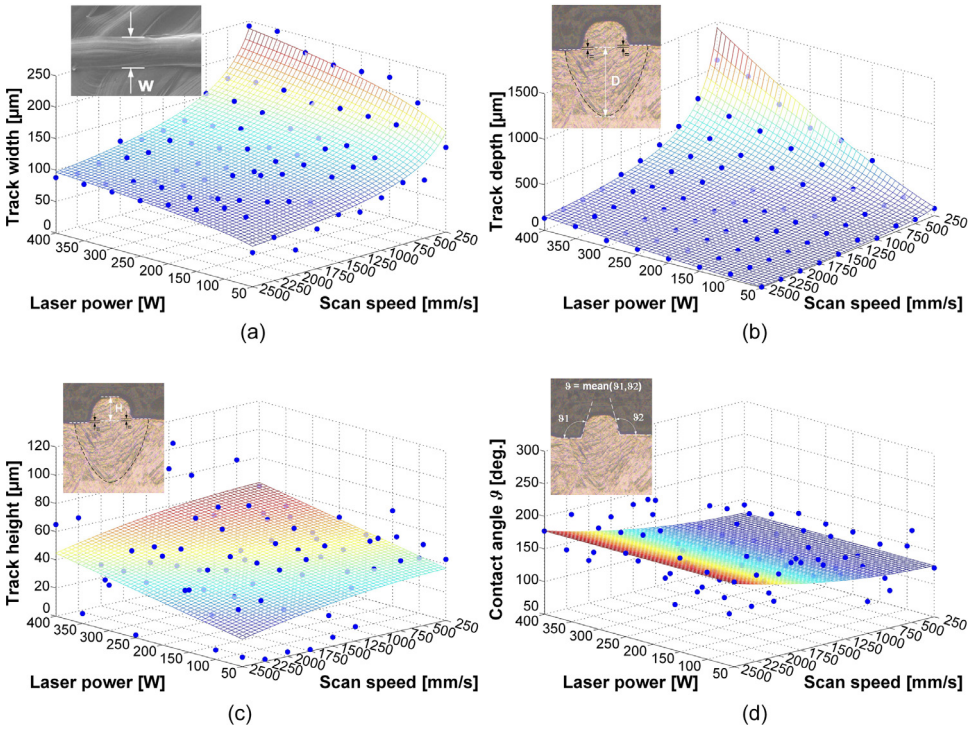

Fig. 5. (a) Width, (b) depth, (c) height, and (d) contact angle of the track. The scan speed axis is oriented from right to left.

750 mm/s. For each of these combinations, microhardness was inspected every 50 µm along the horizontal axis as shown in Fig. 6(c).

The hardness profiles were in agreement with the microstructure of the scan track. No appreciable differences in hardness values were found. The mean hardness corresponded to a Ti martensite phase.

2. Experimental Design, Materials and Methods

The characteristics of the Ti6Al4V powder applied in this research are given in Table 2 and in Fig. 7. The powders were characterized by using a scanning electron microscope (Zeiss Evo 40) equipped with an energy dispersive X-ray spectroscope (INCA X-sight). The grains had a spherical shape (Fig. 7(a)), with diameters ranging from 6.5 µm to 80 µm with a slight negative skewness. The median diameter value was 35.88 µm, whereas the 10^{th} and 90^{th} percentiles were 21.45 µm and 52.19 µm respectively, as illustrated in Fig. 7(b). A sample of the powder was embedded in epoxy resin and underwent metallographic preparation in order to obtain a mirror like surface. Afterwards the specimen was etched by applying Kroll's reagent for 1 min and then

Table 2
Chemical composition of the Ti6Al4V powder used in the process.

Chemical element	Al	V	Fe	O	C	N	H	Ti
Ti6Al4V (% weight)	6.5	4.14	0.18	0.1	0.008	0.007	0.003	89.06

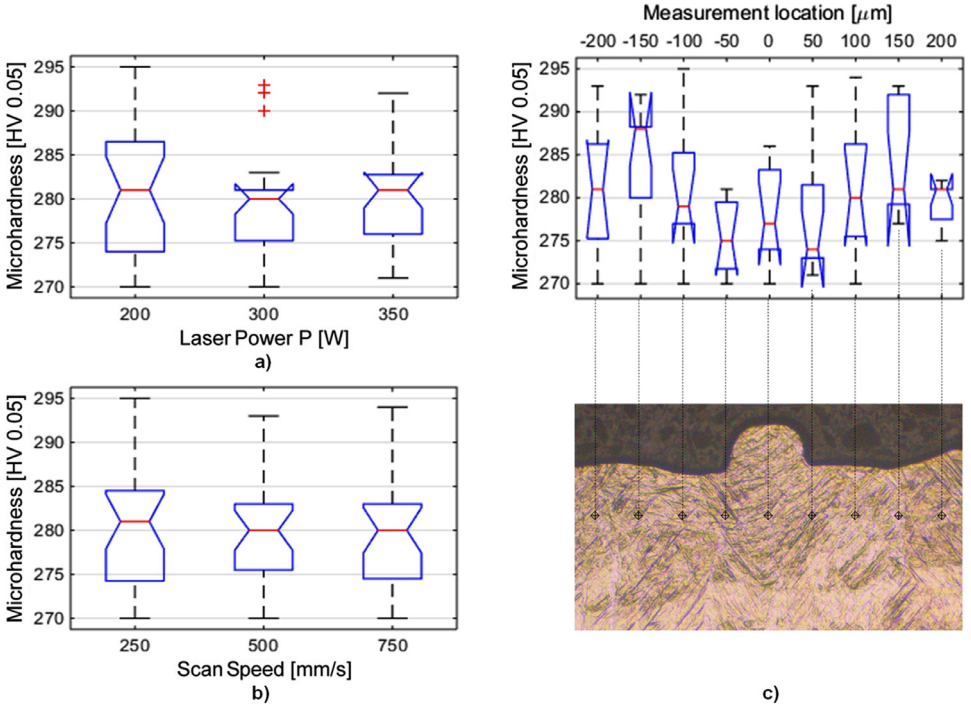

Fig. 6. Microhardness trend with respect to (a) laser power, (b) scanning speed, and (c) measurement location.

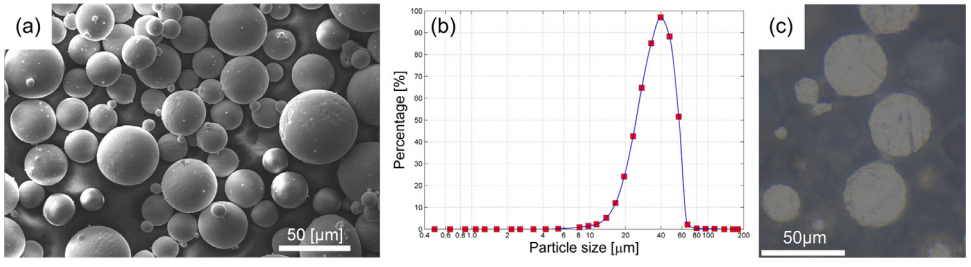

Fig. 7. characterization of Ti6Al4V powders: (a) morphology inspected by SEM; (b) size distribution; (c) metallographic analysis.

analyzed by an Olympus SX-41 optical microscope in order to determine the microstructure of the powders. The microstructure was composed by Ti martensite, obtained by a rapid cooling of molten metal during the production of the spheres, see Fig. 7(c).

The specimens were manufactured with a Concept Laser M2 Cusing machine equipped with a 400 W single-mode CW ytterbium-doped fiber laser. As shown in Fig. 8, the beam intensity had a Gaussian distribution with the beam quality factor $M^2 = 1.08$, and the emission wavelength was 1070 nm. The spot size was regulated to 50 μm, according to the $1/e^2$ classical definition that was also adopted by Xiang et al. in [7]. The optical system of the machine included a Scanlab intelliSCAN 30 two-axis scanning system and a Scanlab varioSCAN$_{de}$ 40i dynamic focusing unit.

Table 3
Process parameters used for the production of the base plates and single tracks.

Parameters	Base plates	Single tracks	Levels
Laser Power	225 W	50 ÷ 400W	8
Scan Speed	1300 mm/s	250 ÷ 2500mm/s	10
Spot Diameter	155 µm	50 µm	1
Layer Thickness	25 µm	25 µm	1
Overlap Rate	40 %	–	–
Scan Strategy	Island	–	–
Replicates	-	–	1

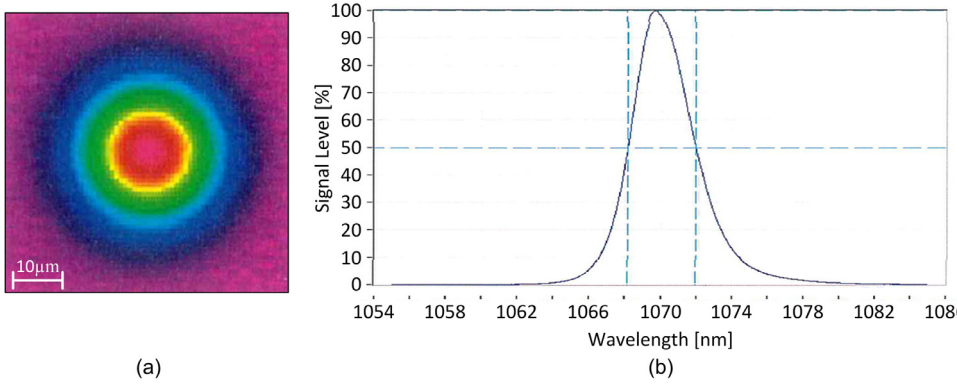

Fig. 8. Properties of the laser used for the experiment: (a) intensity distribution and (b) laser spectrum with respect to the emission wavelength, both measured before the machine's optical system.

Both the laser power and the scan speed were varied in a wide range, as highlighted in the design of experiments shown in Table 3. The layer thickness was 25 µm throughout all the experiments.

All the single tracks were scanned in counterflow with respect to the protective gas flow. This choice was made in order to avoid the interaction between the laser beam and the process fumes, as well as to prevent the precipitation of slags on the material to be processed.

To mimic standard operating conditions, single tracks were printed on the top surface of basic structures that were produced during the previous layers of the same job. All the basic structures were printed by using the same parameters, and top layer passes were set at an angle of 45° with respect to the track direction. The adoption of such bases as single tracks' substrates did considerably simplify the experimental activity by concurrently better reproducing the real process conditions. Single tracks' distribution on such substrates is shown in Fig. 9.

After platform removal the tracks were classified according to their morphology seen from the top by using the same SEM/EDXS device adopted for powder characterization.

Afterwards, all the specimens were cross sectioned by an abrasive refrigerated wheel, embedded in epoxy resin and then ground and polished to obtain a mirror like surface. The last polishing step of the material was done by using colloidal silica. The sections were then etched using Kroll's reagent for 1 min and then analyzed by the optical microscope. Eventually, the cross section microstructure was examined as well as the presence of melting defects (voids, gas porosity, and inclusions) in order to achieve a complete track characterization.

To determine the presence of Heat-Affected Zones in the proximity of the scan track, or of different microstructures between the base and the scan track, a Vickers microhardness profile (load of 0.05 kgf for 15 s) across the scanned track was acquired starting at a depth of 50 µm with respect to the base top surface.

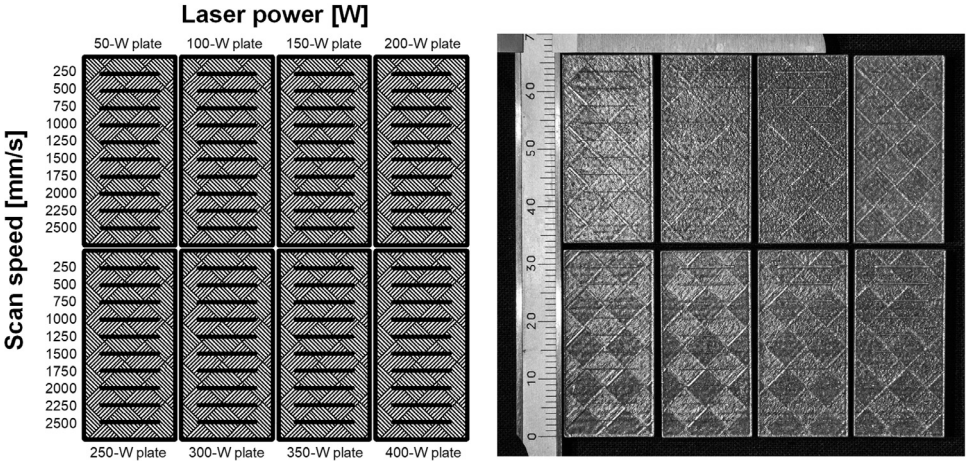

Fig. 9. Design of experiments.

Declaration of Competing Interest

The authors declare that they have no known competing financial interests or personal relationships that could have appeared to influence the work reported in this paper.

Acknowledgments

The Laboratory for Advanced Mechatronics - LAMA FVG - of the University of Udine is gratefully acknowledged for technical support. LAMA FVG is an international research center for product and process innovation where the three Universities of Friuli Venezia Giulia Region (Italy) synergically cooperate for promoting R&D activities at academic and industrial level. The authors are also grateful to M. Magnan and Eng. M. Turco for the technical support during SEM and microstrctural characterization of the specimens.

References

[1] S.Y. Chen, J.C. Huang, C.T. Pan, C.H. Lin, T.L. Yang, Y.S. Huang, C.H. Ou, L.Y. Chen, D.Y. Lin, H.K. Lin, T.H. Li, J.S.C. Jang, C.C. Yang, Microstructure and mechanical properties of open-cell porous ti-6al-4v fabricated by selective laser melting, J. Alloy. Compd. 295 (713) (2017) 248–254.
[2] W. Di, Y. Yongqiang, S. Xubin, C. Yonghua, Study on energy input and its influences on single-track, multi-track, and multi-layer in SLM, Int. J. Adv. Manuf.Technol. 58 (9-12) (2012) 1189–1199.
[3] M. Kniepkamp, J. Fischer, E. Abele, Dimensional accuracy of small parts manufactured by micro selective laser melting, in: Proceedings of the 27th Annual International Solid Freeform Fabrication Symposium 2016, Verlag nicht ermittelbar Austin, TX, 2016, pp. 1530–1537.
[4] C. Li, Y.B. Guo, J.B. Zhao, Interfacial phenomena and characteristics between the deposited material and substrate in selective laser melting inconel 625, J. Mater. Process. Technol. 243 (2017) 269–281.
[5] Q.B. Nguyen, D.N. Luu, S.M.L. Nai, Z. Zhu, Z. Chen, J. Wei, The role of powder layer thickness on the quality of SLM printed parts, Arch. Civ. Mech. Eng. 18 (2018) 948–955, doi:10.1016/j.acme.2018.01.015.
[6] P. Wei, Z. Wei, Z. Chen, J. Du, Y. He, J. Li, Y. Zhou, The alsi10mg samples produced by selective laser melting: single track, densification, microstructure and mechanical behavior, Appl. surf. Sci. 408 (2017) 38–50.
[7] Y. Xiang, S. Zhang, Z. Wei, J. Li, P. Wei, Z. Chen, L. Yang, L. Jiang, Forming and defect analysis for single track scanning in selective laser melting of ti6al4v, Appl. Phys. A 124 (10) (2018) 685.
[8] I. Yadroitsev, P. Krakhmalev, I. Yadroitsava, Hierarchical design principles of selective laser melting for high quality metallic objects, Addit. Manuf. 7 (2015) 45–56.
[9] I. Yadroitsev, I. Smurov, Selective laser melting technology: from the single laser melted track stability to 3d parts of complex shape, Phys. Procedia 5 (2010) 551–560.